GEOPHYSICS, VOL. 71, NO. 4 (JULY-AUGUST 2006); P. B111–B119, 17 FIGS.
10.1190/1.2216189

Application of new seismic attributes to collapse chimneys in the Fort Worth Basin

E. Charlotte Sullivan[1], Kurt J. Marfurt[2], Alfred Lacazette[3], and Mike Ammerman[4]

ABSTRACT

Three-dimensional seismic volumes from the central Fort Worth Basin display roughly circular collapse chimneys that extend vertically about 800 m from the Ordovician Ellenburger Formation to the Atokan (middle Pennsylvanian) Caddo Limestone. Collapse chimneys in carbonates may be caused by subaerial karst, hydrothermal, or tectonic extensional processes. We use 3D multitrace geometric attributes including coherence, volumetric curvature, and energy-weighted, coherent amplitude gradients to investigate details of the origin of these structures. The Ordovician Ellenburger surface resembles a subaerial karst landscape of cockpits, dolines, and frying-pan valleys, while resistivity-based wireline image logs record 50 m of karst breccia facies. However, images from coherence and long-wavelength most-positive and most-negative-curvature volumes show many of the 800-m collapse features are associated with basement faults or with subtle Pennsylvanian and younger tectonic features, rather than with intra-Ellenburger collapse. We hypothesize that although the Ellenburger surface does contain a subaerial karst overprint, the first-order control on the formation of the vertically extensive collapse chimneys is bottoms-up tectonic-induced extensional collapse. Although these collapse chimneys have been affected by burial fluid diagenesis, the main consequence of burial fluid flow may be limited to the documented cementation of macrofractures. The apparent dominance of tectonic extension processes over subaerial karst and hydrothermal processes has basinwide implications for distribution of fractures, late-stage cements, and reservoir development and compartmentalization.

INTRODUCTION

Over one-third of the world's hydrocarbon reserves are in carbonate reservoirs, most of which are fractured, and many of which display collapse features that may vertically extend for 10s to 100s of meters. These collapse features can compartmentalize reservoirs (Bagdan and Pemberton, 2004) and, if they persist as topographic features, may influence the deposition and distribution of reservoir sands and carbonates in younger strata (Hardage et al., 1996). Rounded collapse features (collapse chimneys) in subsurface carbonates may result from subaerial karst processes and cavern collapse, from hydrothermal brecciation and dissolution, from tectonic extension associated with fault movement, or from some combination of these processes (Berger and Davies, 1999; Loucks et al., 2004; Sagan and Hart, 2004; McClay and Borora, 2001). Determining the relative contribution and sequence of each process generating collapse features is important for constructing reservoir models, understanding reservoir performance, and identifying potential for reservoir development related to suprastratal deformation. Data for determining the origin of collapse features include lithology and rock texture from well cuttings, cores and wireline image logs, and geochemical signatures of rock samples. When well data are not available, seismic data are the primary means of identifying the origin and evolution of collapse features. This paper demonstrates the use of multitrace seismic attributes to follow the evolution of vertically extensive collapse features in an area where borehole data are limited.

Volumetric seismic attributes, including coherence, reflector curvature, reflector rotation, and energy-weighted, coherent amplitude gradients provide improved means for imaging small scale and subtle features and tracking changes in these features. In particular, reflector curvature calculated from discrete interpreted horizons is well correlated to fracture intensity (Lisle, 1994; Roberts, 2001), while multispectral estimates of reflector curvature allow interpreters to view long and short wavelength geologic features. In contrast to conventional reflector curvature attributes, multitrace geometric

Manuscript received by the Editor January 6, 2005; revised manuscript received December 8, 2005; published online August 2, 2006.
[1]Pacific Northwest National Laboratories, P.O. Box 999, Richland, Washington 99352. E-mail: charlotte.sullivan@pnl.gov.
[2]502F S&R1, University of Houston, Allied Geophysical Laboratories Houston, Houston, Texas 77204. E-mail: kmarfurt@uh.edu.
[3]Natural Fractures.com LLC, 1302 Waugh Drive, Suite 637, Houston, Texas 77019. E-mail: alfred_lacazette@naturalfractures.com.
[4]Devon Energy Corporation, 20 North Broadway, Oklahoma City, Oklahoma 73102. Email: mike.ammerman@dvn.com.

attributes produce a 3D attribute volume and facilitate the recognition of irregular geologic features by avoiding the need to preinterpret horizons. Well-established coherence attributes measure the lateral changes in waveform, and, as such, are often sensitive to small faults and to lateral changes in stratigraphy such as channels and sinkholes. Estimates of reflector curvature, including most-negative, most-positive, Gaussian curvature, and related shape indices measure the lateral changes in reflector dip and azimuth and are mathematically independent of coherence measures. We have applied coherence and new volumetric, multitrace algorithms to a conventional 3D seismic volume from the Fort Worth Basin of north Texas to test hypotheses on the timing and origin of collapse chimneys that vertically extend from the Ordovician Ellenburger carbonates through Mississippian and Pennsylvanian siliciclastics and carbonates over a distance of almost 800 m.

The Fort Worth Basin is a Paleozoic foreland basin that formed along the advancing border of the Ouachita fold and thrust belt (Figure 1), associated with the oblique lithospheric convergence of the North American and South American plates (Walper, 1982). The lower Ordovician Ellenburger carbonates (Figure 2) were deposited in a shallow ramp setting and are unconformably overlain by upper Ordovician Viola Limestones (missing because of erosion in our area). The overlying organic-rich Barnett Shale records deposition in the developing deep-water foreland basin during the late Mississippian. Shallow-water siliciclastics and carbonates of the Marble Falls and Caddo record basin filling during the early to middle Pennsylvanian (Walper, 1982; Montgomery et al., 2005). The Ellenburger, in the area of seismic coverage, underwent at least two extensive episodes of subaerial weathering that may have produced karst landscape and cavern systems. The first episode occurred during the middle Ordovician and is associated with a cratonwide regional unconformity following the Ellenburger deposition (Kerans, 1990; Franseen et al., 2003). The second episode of exposure is less well constrained, but aerially covered much of north-central Texas and occurred during the Mississippian development of the Fort Worth Basin. Silurian and Devonian strata are missing over the study area, along with any sedimentary record of possible additional times of exposure (Grayson and Merrill, 1991; Bowker, 2003).

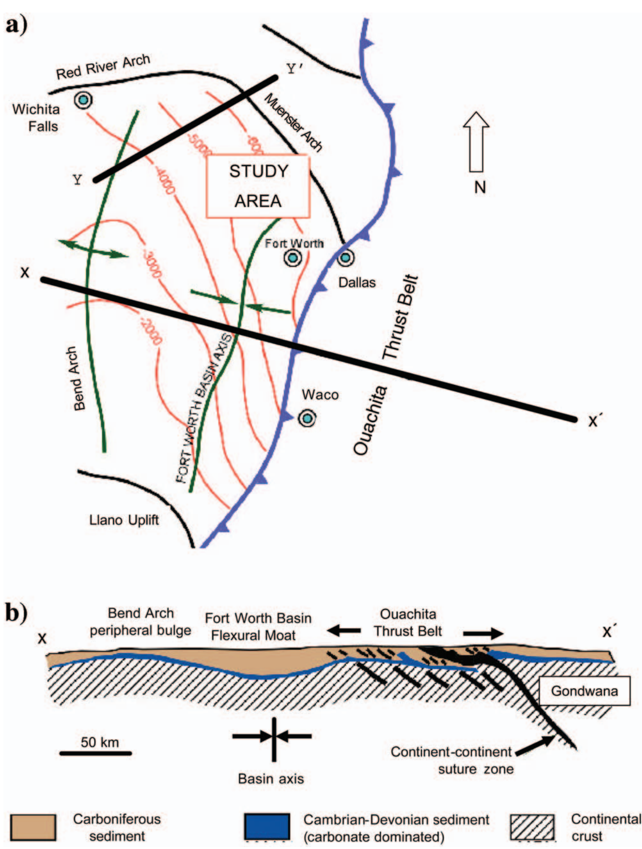

Figure 1. The Fort Worth Basin and the Pennsylvanian Ouachita thrust belt. The basin developed as a foredeep and underwent compression and strike-slip deformation during the Pennsylvanian, followed by Mesozoic and Cenozoic extension. Collapse breccias compartmentalize Pennsylvanian reservoirs in the shaded area (after Hardage et al., 1996).

In addition to being karsted, the Ellenburger underwent a number of postburial tectonic events, including compression and oblique slip associated with late Paleozoic continental collision and the westward advancing Ouachita orogen (Ball and Perry, 1996) and late extension related to the Mesozoic opening of the Gulf of Mexico and the later formation of the regional down-to-the-coast Miocene Balcones fault system (Hoskins, 1982). We anticipate that seismic attributes and conventional seismic volumes may reveal temporally different karst and tectonic overprints associated with these events.

Karst terrains contain geomorphic features such as sinkholes, cockpit landforms (Cansler and Carr, 2001), and round-ended frying-pan valleys. Cave and potential collapse systems most commonly develop at or above water tables, generally within the upper 100 m of an exposed carbonate surface (Kerans, 1990). Most of the buried Ellenburger cave systems of west Texas collapsed prior to the end of the Ordovician, as evidenced by the age of their fill. Associated cave fill deposits contain Ellenburger breccias and stratified deposits of the transgressive Upper Ordovician Simpson sandstones that regionally overlie the Ellenburger. Irregular Ellenburger topography often is filled completely by the first 20–50 m of Simpson

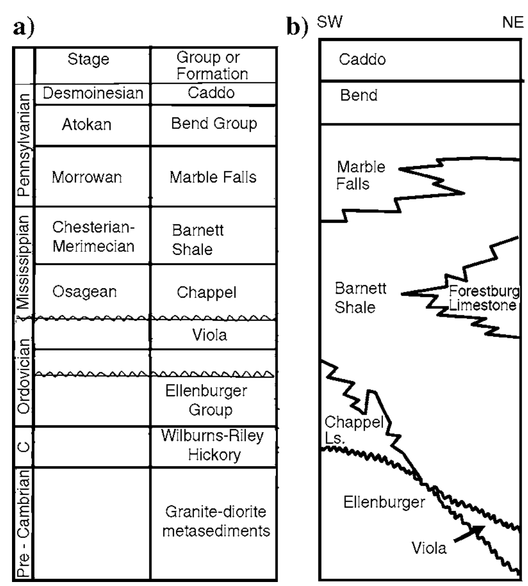

Figure 2. (a) Stratigraphic interval affected by collapse features and (b) southwest-northeast diagrammatic cross section from the Bend Arch to the Muenster Arch, along line Y-Y′ in Figure 1. The Forestburg carbonates appear to be shed from shallow water environments on the Muenster Arch (after Pollastro, et al., 2003).

deposition (Kerans, 1990). In contrast, the collapse chimneys in our data persist through about 800 meters of section. Collapse chimneys of similar vertical extent also are present above the Ellenburger to the west of our study area (Hardage et al., 1996).

The character of the vertical collapse features in the Fort Worth Basin may record a complex history, similar to the history interpreted by Lucia (1996) for outcrops at the McKelligon Sag, near El Paso, Texas. These outcrops record a vertical collapse system of 760 m that includes collapse of separate Ordovician, Silurian, and Devonian cave systems over a period of 100 million years. Once collapse ended, the surface topography quickly healed; only about 16 m of sediments was required to fill the irregular surface. Isotope data from saddle dolomite in fractures between the McKelligon collapse breccia blocks indicate cement precipitation from deep burial fluids during the Pennsylvanian (Kupecs and Land, 1991). They proposed that the source and migration of these deep burial fluids is related to the emplacement of the Ouachita thrust belt.

This paper sheds light on the possible causes and history of the collapse features in the Fort Worth Basin through the application of modern seismic attributes. We begin with a brief overview of the seismic data quality and geometric attributes. We then examine the geology in the survey area by integrating our new tools with more conventional time/structure and isochore maps. Finally, we use these new images to support our hypothesis that the collapse features are controlled more by tectonics than by subaerial karst or thermobaric processes. We propose that the collapse chimneys are extensional fault-related, polygonal depressions (rhombochasms), affecting basement and higher strata and, that these chimneys have been reactivated by multiple tectonic events.

METHODOLOGY

The seismic survey used in this study is a composite of three separate acquisition programs. The data were acquired and processed by a petroleum company through a commercial vendor using a workflow that consisted of elevation and static corrections, deconvolution, dip moveout, stack, and poststack time migration. This poststack data volume (Figure 3a) was then subjected to the attribute analysis described in this paper. First we applied edge-preserving principal-component filtering (Marfurt, 2006) to suppress random noise and enhance subtle discontinuities and offsets at minor faults (Figure 3b). We note that the impact on the waveform and amplitude is minimal but that the terminations are sharper.

Next we calculated a complete suite of geometric seismic attribute volumes on both the original and edge-enhanced seismic data, including coherence (Marfurt et al., 1999), multispectral curvature and energy-weighted, coherent amplitude gradients (Marfurt, 2006). We also tied wells and performed poststack impedance inversion and generated more conventional single-trace attributes. These attribute cubes were loaded into an interpretation workstation and interpreted along with the seismic data and well control. The coherence, dip/azimuth, and energy-weighted, coherent-amplitude gradient volumes were generated using nine overlapping nine-trace, ±10 ms analysis windows. The multispectral curvature and rotation volumes were calculated using circular analysis windows containing between 13 traces (for short wavelength calculations) and 78 traces (for long wavelength calculations). The principal-component filtered version of the data was more amenable to automatic picking. Of all the attributes calculated, we found the long wavelength most-positive and most-negative curvature, energy-weighed, coherent amplitude gradients, and principal-component estimate of coherence were the most valuable for our interpretation of faults, fractures, and karst features. However, we must emphasize that these high-tech attributes were only fully understood and are best communicated when integrated into the conventional interpretation work flow of tying wells, generating time/structure maps, generating isochores, and producing horizon extractions.

DATA ANALYSIS

In Figure 3b we indicate faults and some of the major horizons of interest in this study. Collapse features extend from within the Precambrian basement (yellow) through the Ordovician Ellenburger (green), early Pennsylvanian Marble Falls (magenta) and middle Pennsylvanian Caddo Limestone (cyan). The Atoka horizon marks the top of a sand/siltstone sequence that has been a prolific producer, enhanced by thicker sands filling in the collapse features. We plot faults that penetrate the deeper part of the section in orange and those that are limited to the shallower section in yellow. A regional wrench fault system crosses the survey near the white arrow, close to A. The

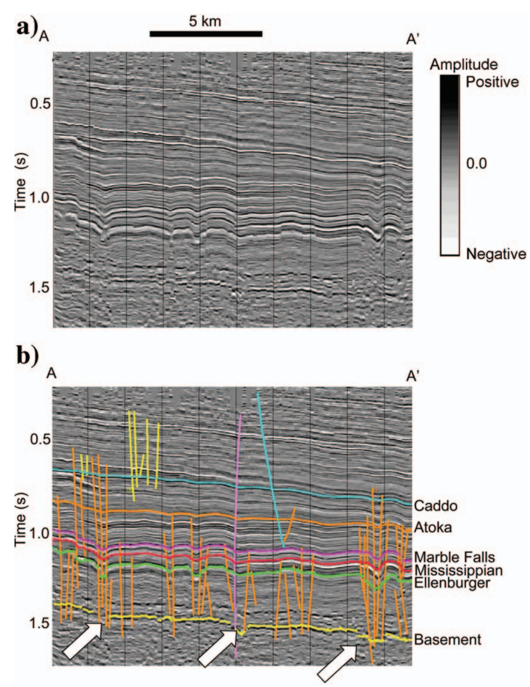

Figure 3. North-south line AA′ through the maps shown in Figures 4 and 5, (a) without and (b) with interpretation. We have applied edge-preserving principal component filtering to these data. The cyan horizon is the Pennsylvanian Caddo limestone; The green Ellenburger pick is Lower Ordovician. Note the vertical collapse features indicated by the white arrows. These collapse features are not filled in immediately above the Ellenburger but can be tracked from the basement to shallower events. Orange faults penetrate the basement; yellow faults are confined to strata above the basement. The magenta fault is the major fault crossing the center of the survey.

magenta fault is subtler but has components of dip, and perhaps, strike slip as well. The wrench fault, the magenta fault, and the collapse features are evident on the time structure maps of the Marble Falls (Figure 4a) and Ellenburger (Figure 4b). The time isochore between the Ellenburger and Marble Falls (Figure 5a) indicates a fairly uniform pattern, with thicker fill in the collapse feature and thickening north of the magenta fault. In contrast, the time isochore for the Marble Falls–Atoka interval (Figure 5b) displays a strong northeast-southeast and southwest-northeast blocky fabric. Time slices through the coherence volume (Marfurt et al., 1999) at the Marble Falls (Figure 6a) and Ellenburger (Figure 6b) levels show a complex system of lineaments and collapse features. Although horizon extractions of coherence are particularly valuable for mapping smooth stratigraphic features, time slices provide a less biased view of irregular or rugose surfaces. Although we do see the vertical trace of several faults, the most prominent features are the circular collapse features, which are more pronounced at the deeper Ellenburger level than at the Marble Falls level. These collapse features are aligned in conjugate northeast-southwest and northwest-southeast trends, and some are quite elongated, rather than circular. To understand these collapse patterns and their expression in the curvature attributes, we display a folded section (Figure 7) through the filtered vertical seismic cube corresponding to line AA′ in Figure 6, coupled with a time slice at 1.2 s through the original seismic volume. We then compare this image to time slices of 1.2 s through the most-negative and most-positive curvature attribute volumes.

To facilitate this comparison, we construct multiattribute displays (Figures 8 and 9), where the original seismic data are shown on the vertical face. Remember that although the value of the most-negative curvature is always less than the value of the (orthogonal) most-positive curvature at any analysis point, both attributes can have negative values (for a bowl), and both attributes can have positive values (for a dome). Examining Figures 8 and 9 confirms this relation. Features that are bowls (collapse features) will have a negative value of positive curvature, colored green in Figures 8a and 9a. Features that are domes will have a positive value of negative curvature and are red in Figures 8b and 9b. Lineaments in the most-negative curvature time slices can usually be interpreted as valleys, while lineaments on the most-positive curvature usually can be interpreted as ridges. We note in Figures 8 and 9 that our collapse features often are linked together, suggestive of cockpit karst and karst collapse features described in Figures 10 and 11. Although we expect there is a

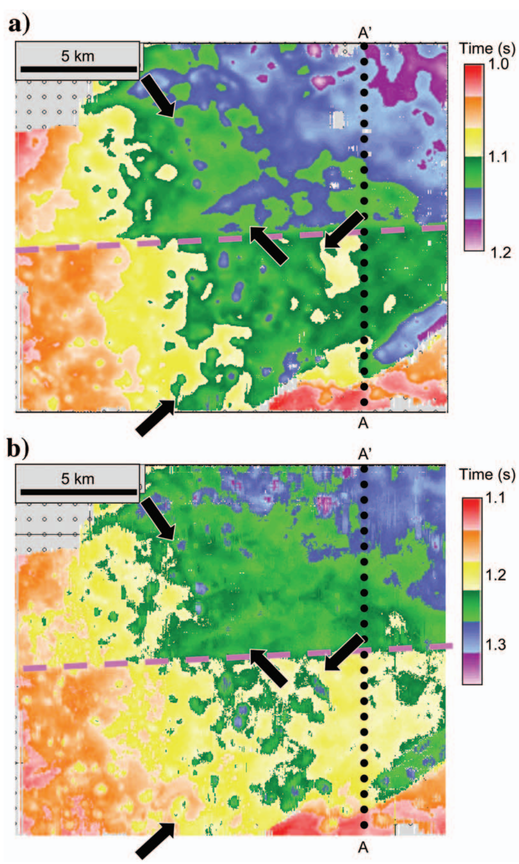

Figure 4. Time structure maps on the (a) Marble Falls and (b) Ellenburger horizons. Arrows are shown in Figure 5 for reference. Line AA′ is shown in Figure 3.

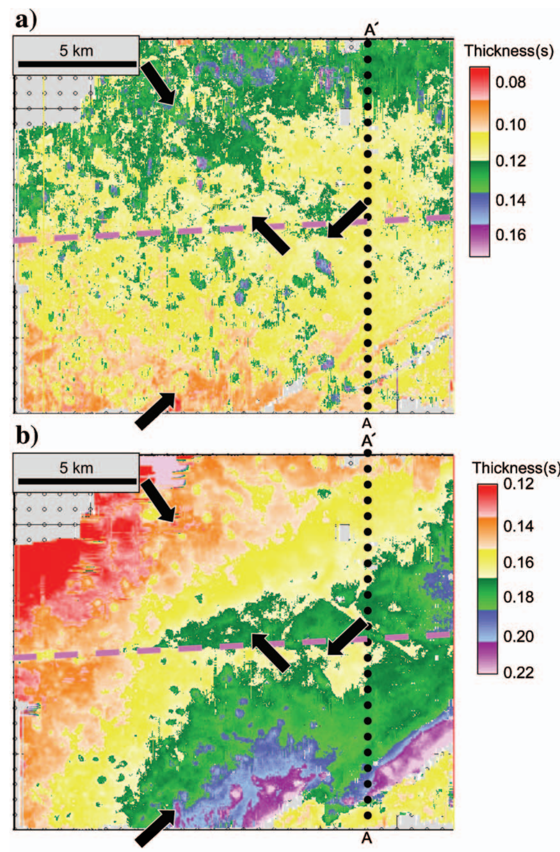

Figure 5. Isochore (time-thickness) maps between (a) the Ellenburger and Marble Falls horizons and (b) Marble Falls and Atoka horizons. Line AA′ is shown in Figure 3. Arrows are identical to those in Figures 3 and 4 showing collapse features. We note that we still observe differential thickness corresponding to continued collapse after Marble Falls deposition.

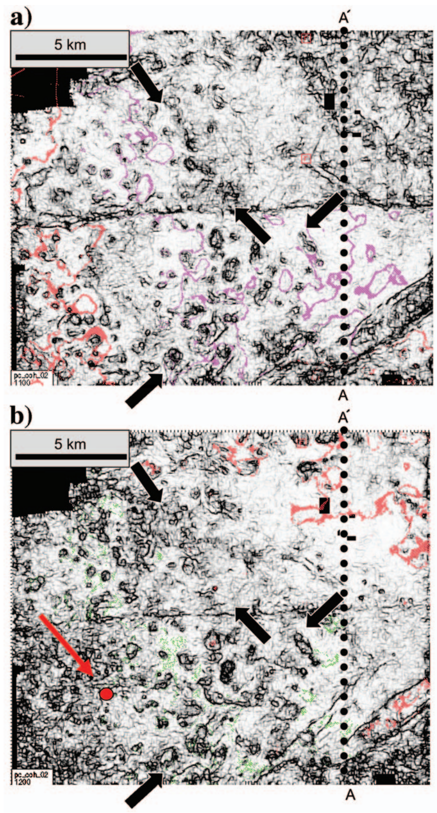

Figure 6. Time slices through the coherence volume at (a) 1.1 s and (b) 1.2 s. Note the Marble Falls (magenta), Mississippian shale (red) and Ellenburger (green) picks. Black arrows indicate collapse features shown in Figures 3–5. Red arrow locates a cored Ellenburger well.

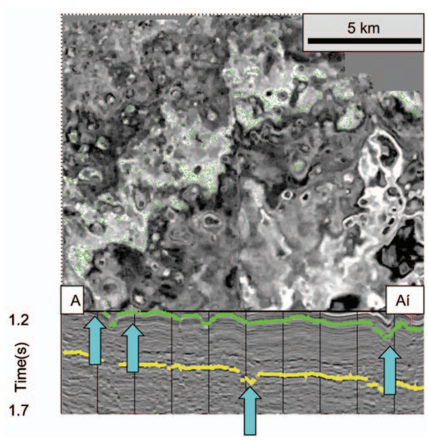

Figure 7. Foldaway view through the seismic data volume along line AA′ shown in Figures 3–6. Top slice is at 1.2 s. The green pick is the Ordovician Ellenburger. The yellow pick is approximate basement. Evidence of downthrown blocks continues into the basement (cyan arrows). Subaerial karst should originate within the Ellenburger, not in the crystalline basement. The seismic data shown here have been enhanced through the use of principal component, edge-preserving filtering.

subaerial karst component to the polygonal features observed in the seismic data, some of the collapse features extend into the Precambrian igneous basement, where karst processes cannot operate.

Time slices at 0.8 s (near top Caddo), 0.9 s, 1.0 s, 1.1 s (near top Marble Falls) 1.2 s (near top Ellenburger) and 1.3 s through the coherence volume (Figure 12), most-negative-curvature volume (Figure 13) and most-positive-curvature volume (Figure 14) provide unique views of the data. The most-negative- and most-positive-curvature attributes clearly image the fault crossing the center of the survey, the regional wrench fault in the southeast of the survey, and a complex system of northwest-southeast and northeast-southwest conjugate faults and joints. The coherence image illuminates the edges of the individual karst features but gives little direct indication of their linkage nor of the small offset faults that are clearly seen on Figures 3a and b. A dual gradational color bar is particularly effective for curvature analysis so that we see red domal features bounded

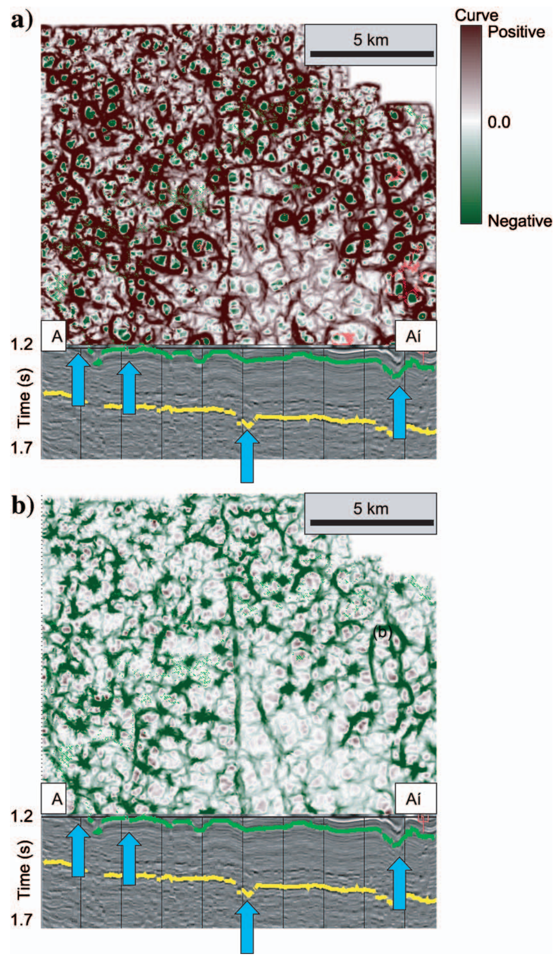

Figure 8. Foldaway combined attribute images corresponding to Figure 7. Seismic data are displayed on the vertical face. Long-wavelength (a) most-positive curvature and (b) most-negative curvature are shown on the time slices. Positive values (red) on the most-negative curvature slice correspond to domes, while negative values (green) on the most-positive curvature slice correspond to bowls. We interpret such bowls as tectonic collapse features, linked by a complex system of faults and joints.

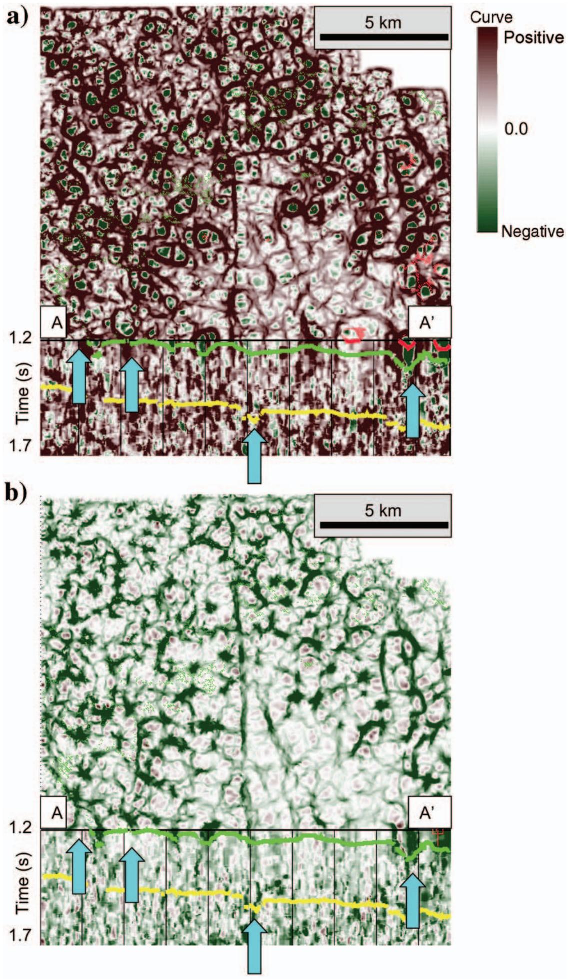

Figure 9. Foldaway long-wavelength curvature images corresponding to Figures 6 and 7: (a) most-positive curvature and (b) most-negative curvature. Curvature attributes are displayed on the vertical face. Curvature calculations were performed on a circular grid containing 75 traces a vertical analysis window of ± 10 ms to minimize vertical smearing. We note consistent patterns of curvature with depth, cutting through the basement (yellow) pick. Some of these curvature features appear to be non vertical (arrows) implying they are controlled by faults.

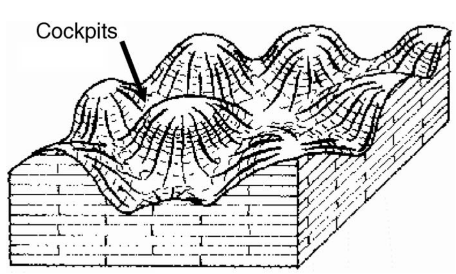

Figure 10. Mature cockpit karst topography results from a combination of dissolution and preburial collapse of cave systems. In this process, well cemented, low-porosity intercave areas persist as rounded knolls and hills (after Cansler and Carr, 2001).

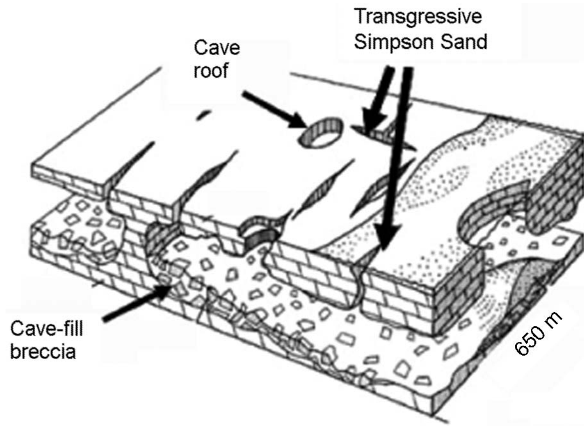

Figure 11. Karst model of features associated with subaerial weathering and erosion of West Texas Ellenburger carbonates. Cave systems most commonly fill with collapse breccias and sediments associated with subsequent marine transgressions (after Kerans, 1990).

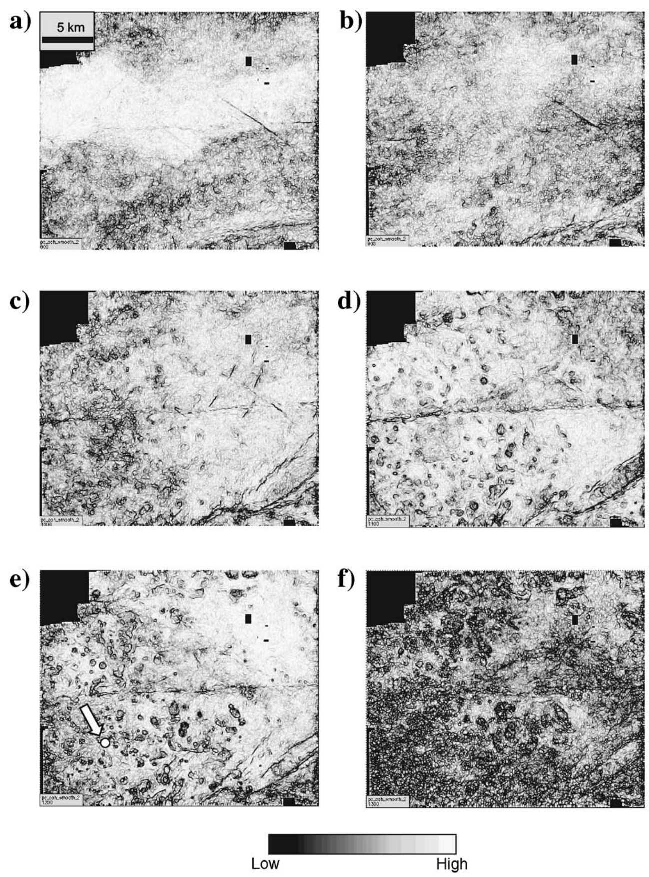

Figure 12. Slices through the coherence volume at (a) 0.8 s, (b) 0.9 s, (c) 1.0 s, (d) 1.1 s, (e) 1.2 s, and (f) 1.3 s. The analysis window is ± 10 ms and 9 traces. White arrow in Figure 12e indicates location of image log shown in Figure 15.

by green valleys on the most-negative-curvature attribute (Figure 13) and green collapse features between red ridges on the most-positive-curvature attribute (Figure 14).

We also note that the collapse features appear to be most intense (sharpest) below the Ellenburger horizon in Figures 12e, 13e, and 14e and gradually broaden to the Caddo horizon in Figures 12a, 13a, and 14a. Although we feel confident that the Ellenburger has undergone subaerial karst generation, as evidenced by distinctive karst breccia facies in an image log (Figure 15) from the study area, we observe this is a pervasive background overprint. The location of the well in Figure 15 is marked in Figure 12e (white arrow), and is not associated with a large collapse feature. We note a marked change in the distribution of lineaments with age, which we show as rose diagrams in Figure 16. While the collapse features appear to be pervasive from basement to above the Caddo horizon, the tectonic stresses have changed direction over geologic time.

We have found in other surveys (Blumentritt et al., 2003) that the energy-weighed, coherent amplitude gradient can be effective in delineating lateral changes in rock thickness, which are often expressed in seismic data as changes in thin bed tuning. The energy-

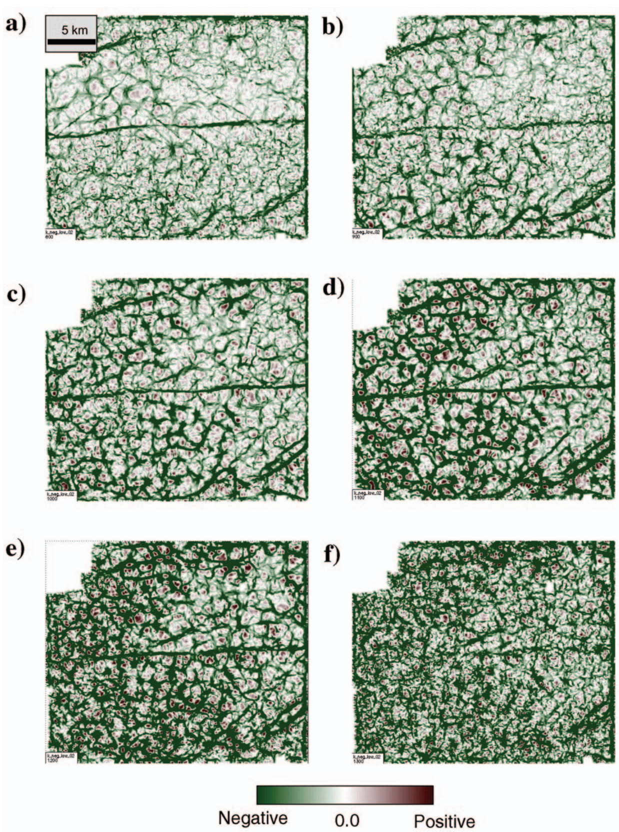

Figure 13. Slices through the most-negative-curvature volume at (a) 0.8 s, (b) 0.9 s, (c) 1.0 s, (d) 1.1 s, (e) 1.2 s, and (f) 1.3 s. We used a long-wavelength calculation with an analysis window of ±10 ms and 75 traces. Color bar is identical to those used in Figures 8 and 9. Domes appear brown. Bowls and valleys appear green. Note persistence of collapse features with depth and lack of lateral offset of features along post-Caddo east-west fault.

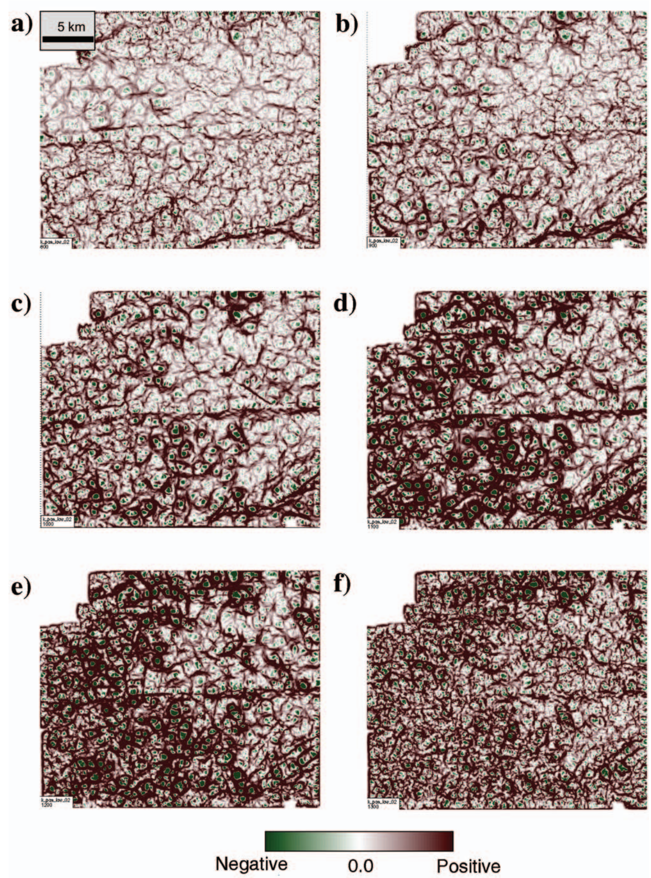

Figure 14. Slices through the most-positive-curvature volume at (a) 0.8 s, (b) 0.9 s, (c) 1.0 s, (d) 1.1 s, (e) 1.2 s, and (f) 1.3 s. We used a long-wavelength calculation with an analysis window of ±10 ms and 75 traces. Color bar is identical to those used in Figures 8 and 9. Bowls (collapse features) are green. Domes and ridges are brown.

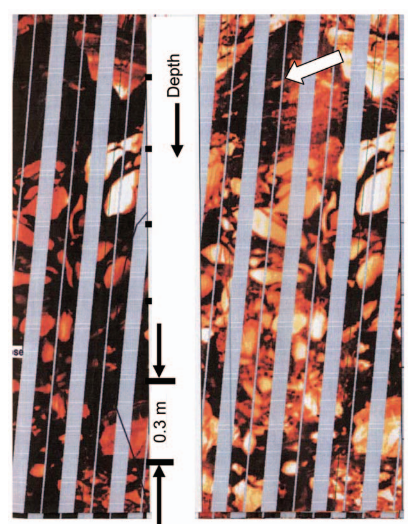

Figure 15. Resistivity-based image log showing karst breccia fabric, including rounded plus angular matrix-supported clasts and stratified fine sediment (white arrow). Location of well is indicated by arrow in Figure 12e; note that well location is not within a major collapse feature (data courtesy of Devon Energy).

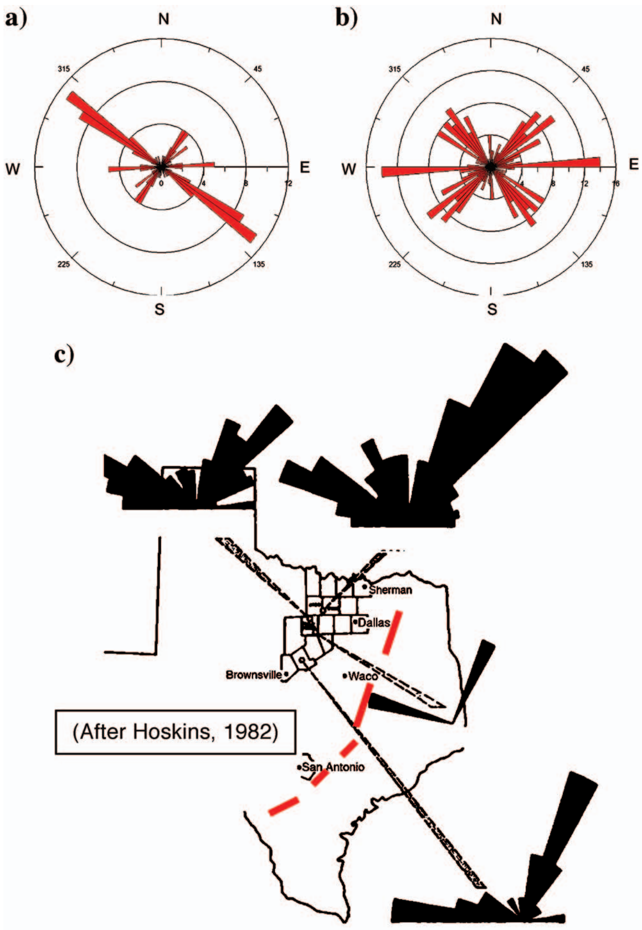

Figure 16. Rose diagrams of lineaments. Picked on time slices at (a) approximately top of the Caddo horizon at 0.8 s, as shown in Figures 12a, 13a, and 14a and (b) at approximately the top of the Ellenburger horizon as shown in Figures 12e, 13e, and 14e. Hoskins (1982) measured joints in surface outcrops (c) near the study area and related these to Miocene extension along the Balcones fault system (red lines). Present-day maximum stress σ_1 is vertical in the subsurface study area, and σ_2, the maximum horizontal stress, is N40–47°E (after Siebrits et al., 2000).

weighted, coherent amplitude gradients extracted along the Ellenburger horizon (Figure 17) show three types of features. The first type of feature, indicated by yellow arrows, has a craterlike appearance. These craters correspond to the location of collapse structures seen on the Ellenburger coherence volume (Figure 12e) and to local thickening on the Ellenburger-Marble Falls isochore map (Figure 5). We interpret these features as resulting from changes in sediment thickness within the collapse structures. The second type of feature, indicated by magenta arrows on the energy-weighted, coherent amplitude attribute image, are linear events that correlate well with faults and fractures seen in the other attribute volumes. The third type of feature, indicated by green arrows, is not apparent on any of the other attribute extractions or time slices. We interpret these features as thin meandering channels that appear to be controlled by the valleys and collapse features seen in Figure 13e. Other, more diffuse features we interpret as tuning effects associated with filling these valleys.

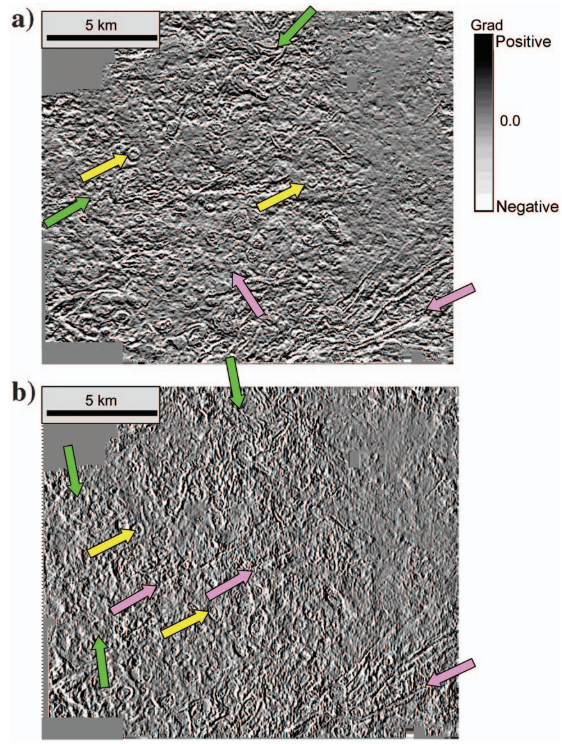

Figure 17. (a) North-south and (b) east-west energy-weighted, coherent amplitude gradient extracted along the Ellenburger horizon. Yellow arrows indicate representative circular collapse features; magenta arrows indicate lineations associated with faults and fractures, and green arrows indicate meandering channels and in-filled paleo topography. Subtle NS striations in (b) are attributable to acquisition footprint.

CONCLUSIONS

While the horizontal expression of the vertical collapse features in the Fort Worth Basin data is readily seen on traditional time/structure and isochore maps (Figures 4 and 5), their relationship to faulting is more clearly presented in time slices and horizon extractions through coherence and curvature attribute volumes (Figures 12–14). We note that the collapse features are intense at the Ellenburger time and cut into the basement in some areas but are greatly subdued at the Caddo Limestone level (Figures 12–14). Indeed, the expression at Caddo time (Figure 12a) shows no discontinuities, implying that the collapse seen on the curvature volumes (Figures 13a and 14a) is attributable to either continued compaction or dissolution from below, rather than to top-down, subaerial karst processes following deposition of the Caddo.

Isochrons of Marble Falls to Ellenburger (Figure 5a) and Caddo to Marble Falls (Figure 5b) show decreasing magnitude of the circular collapse features, demonstrating that collapse was episodic and decreasing by Atokan time. The alignment of collapse features at the deeper levels (Figures 12e–14e) with shallow lineaments suggests a post-Atokan reactivation of those joints. Current maximum stress in the subsurface Mississippian strata near the study area is vertical; in the area of seismic coverage, the stress σ_2 is N40-47E. Within the study area, open joint systems in surface outcrops of the Upper Pennsylvanian are dominated by NNE and NNW sets (Figure 16c), which Hoskins (1982) interprets as related to extension along the trans Texas Miocene-age, down-to-the-coast Balconies fault system (although we speculate there may be Mesozoic extension as well). We interpret the observed features in the seismic data as indicating that Ellenburger subaerial karst events were influenced by basement faults, and that these faults were reactivated during deposition of Atokan siliciclastics. Orientation of pinnate lineaments at the Ellenburger level and extensional joints at the Caddo level suggest possible reversal of stresses in the area related to the Ouachita orogeny and later Miocene or other extensional events.

We conclude that some of the collapse features originated as subaerial karst, as evidenced by channels cutting the top of the Ellenburger (Figure 17) and that karst formation was likely more intense below the Mississippian unconformity than below the middle Ordovician unconformity. We have observed that in other Fort Worth Basin 3D surveys that Lower Ordovician Ellenburger carbonates overlain by Upper Ordovician carbonates appear to contain a lower density of sinkholelike features than do Ellenburger carbonates overlain directly by Mississippian shales.

Although the Ellenburger carbonates were subaerially exposed at least twice, we propose that most of the extensive collapse chimneys observed in the seismic volume is the result of extensional faulting, enhanced, perhaps, by deep burial fluids moving along Pennsylvanian or younger fractures and seismic-scale faults. Calcite cement plugging of macrofractures observed within the Mississippian shales may represent a final stage of this process.

We anticipate that further improvements in the attributes that we have used will allow us to further separate subtle faults and collapse features that form under different conditions. For example, we expect that differences in timing and mode of karst formation have the potential to produce cave fill and plumbing systems with distinct patterns of porosity and permeability. The geomorphic expression of karst or tectonic collapse features is increasingly recognized as an important control on the deposition and fracturing of younger reservoirs for the Fort Worth Basin and for sandstones above karsted Mississippian carbonates in Kansas. We believe that the application of such new seismic attributes to 3D seismic volumes allows detection of normally subseismic features and provides a tool for determining timing and nature of features that may be related to karst, tectonic, or hydrothermal collapse and for improved mapping of reservoir bodies, permeability fairways, and various surfaces associated with weathered and fractured carbonates.

ACKNOWLEDGMENTS

We wish to thank the United States Department of Energy DE-FC26-04NT15504 and the sponsors of the Allied Geophysical Laboratory Consortium for financial support of research. We particularly thank Devon Energy for permission to use its data.

REFERENCES

Bagdan, C. A., and S. G. Pemberton, 2004, Karst breccia and bank collapse breccia: Implications for reservoir characterization of the McMurray Formation, Alberta, Canada: AAPG Bulletin, **88**, 13.

Ball, M. M., and W. J. Perry, 1996, Bend Arch-Fort Worth Basin Province: U. S. G. S. Report for Province 45.

Berger, Z., and G. Davies, 1999, The development of linear hydrothermal dolomite (HDT) reservoir facies along wrench or strike slip fault systems in the Western Canadian Sedimentary Basin: Canadian Society of Petroleum Geologists Reservoir, 34–38.

Blumentritt, C. H., K. J. Marfurt, and E. C. Sullivan, 2003, Limits to seismic resolution of stratigraphic features-Applications to the Devonian Thirty-one Formation, Central Basin Platform, in T. J. Hunt, and P. H. Lufholm, eds., The Permian Basin, back to the basics: West Texas Geologic Society Publication 03–112, 209–218.

Bowker, K. A., 2003, Recent developments of the Barnett Shale Play, Fort Worth Basin: West Texas Geological Society Bulletin, **42**, 4–11.

Cansler, J. R., and T. R. Carr, 2001, Paleogeomorphology of the sub-Pennsylvanian Unconformity of the Arbuckle Group (Cambrian-Lower Ordovician): Kansas Geological Survey, open file report 2001–55.

Franseen E. K., A. P. Byrnes, J. Cansler, D. M. Steinhauff, T. R. Carr, and M. K. Dubois, 2003, Geologic characteristics of Arbuckle reservoirs in Kansas: Proceedings of the 15th Oil Conference, Tertiary Oil Recovery Project, The University of Kansas, 28.

Grayson, R. C., and G. K. Merrill, 1991, Carboniferous geology and tectonic history of the Southern Fort Worth (foreland) Basin and Concho Platform, Texas: GSA Field Trip Guidebook: Dallas Geological Society, 67.

Hardage, B. A., D. L. Carr, D. E. Lancaster, J. L. Simmons, Jr., R. Y. Elphick, V. M. Pendelton, and R. A. Johns, 1996, 3-D Seismic evidence for the effects of carbonate karst breccia collapse on overlying clastic stratigraphy and reservoir compartmentalization: Geophysics, **61**, 1336–1350.

Hoskins, B. W., 1982, Fracture analysis of Pennsylvanian carbonate bank systems in the Graford Formation North Central Texas, *in* C. A. Martin, ed., Petroleum geology of the Fort Worth Basin and Bend Arch area: Dallas Geological Society, 179–192.

Kerans, C., 1990, Depositional systems and karst geology of the Ellenburger Group (Lower Ordovician), subsurface West Texas: The University of Texas at Austin, Bureau of Economic Geology Report of Investigations, 193, 63.

Kupecs, J. A., and L. S. Land, 1991, Late Stage dolomitization of the Lower Ordovician Ellenburger Group, west Texas: Journal of Sedimentary Petrology, **61**, 551–574.

Lisle, R. J., 1994, Detection of zones of abnormal strains in structures using Gaussian curvature analysis: AAPG Bulletin, **78**, 1811–1819.

Loucks, R. G., P. K. Mescher, and G. A. McMechan, 2004, Three-dimensional architecture of a coalesced, collapsed-paleocave system in the Lower Ordovician Ellenburger Group, central Texas: AAPG Bulletin, **88**, 545–564.

Lucia, F. J., 1996, Lower Paleozoic cavern development, collapse, and dolomitization, Franklin Mountains, El Paso, Texas *in* E. Stoudt, ed., Precambrian-Devonian geology of the Franklin mountains, west Texas- analogs for exploration and production in Ordovician and Silurian reservoirs in the Permian Basin: West Texas Geological Society 1996 Guidebook, 175–196.

McClay, K., and M. Borora, 2001, Analog models of restraining stepovers in strike-slip fault systems: AAPG Bulletin, **85**, 233–260.

Marfurt, K. J., 2006, Robust estimates of 3D reflector dip and azimuth: Geophysics, (this issue).

Marfurt, K. J., V. Sudhakar, A. Gersztenkorn, K. Crawford, and S. Nissen, 1999, Coherency calculations in the presence of structural dip: Geophysics, **64**, 104–111.

Montgomery, S. L., D. M. Jarvie, K. A. Bowker, and R. M. Pollastro, 2005, Mississippian Barnett Shale, Fort Worth basin, north-central Texas: Gas-shale play with multi-trillion cubic foot potential: AAPG Bulletin, **89**, 155–175.

Pollastro, R. M., R. J. Hill, D. M. Jarvie, and M. E. Henry, 2003, Assessing undiscovered resources of the Barnett-Paleozoic Total Petroleum System, Bend Arch-Fort Worth Basin Province, Texas: Transactions of the Southwest Section, AAPG Convention, AAPG/Datapages, CD-ROM 18.

Roberts, A., 2001, Curvature attributes and application to 3D interpreted horizons: First Break, **19**, 85–99.

Sagan, J., and B. Hart, 2004, Seismic and structural analysis of a Trenton-Black River hydrothermal dolomite reservoir: AAPG Search and Discovery Article #40129.

Siebrits, E., J. L. Elbel, R. S. Hoover, I. R. Diyashev, R. T. Holditch, L. G. Griffin, S. L. Demetrius, C. A. Wright, B. M. Davidson, N. P. Steinsberger, and D. G. Hill, 2000, Refracture reorientation enhances gas production in the Barnett Shale tight gas sand: SPE 2000 Annual Technical Conference and Exhibition, SPE paper 63030, 5.

Walper, J., 1982, Plate Tectonic evolution of the Fort Worth Basin, *in* C. A. Martin, ed., Petroleum geology of the Fort Worth Basin and Bend Arch area: Dallas Geological Society, 237–251.